



**HAL**  
open science

# Computation of flexoelectric coefficients of a MoS<sub>2</sub> monolayer with a model of self-consistently distributed effective charges and dipoles

Yida Yang, Laurent Hirsinger, Michel Devel

► **To cite this version:**

Yida Yang, Laurent Hirsinger, Michel Devel. Computation of flexoelectric coefficients of a MoS<sub>2</sub> monolayer with a model of self-consistently distributed effective charges and dipoles. *The Journal of Chemical Physics*, 2022, 156 (17), pp.174104 (11). hal-03889494

**HAL Id: hal-03889494**

**<https://hal.science/hal-03889494v1>**

Submitted on 8 Dec 2022

**HAL** is a multi-disciplinary open access archive for the deposit and dissemination of scientific research documents, whether they are published or not. The documents may come from teaching and research institutions in France or abroad, or from public or private research centers.

L'archive ouverte pluridisciplinaire **HAL**, est destinée au dépôt et à la diffusion de documents scientifiques de niveau recherche, publiés ou non, émanant des établissements d'enseignement et de recherche français ou étrangers, des laboratoires publics ou privés.

1 **Computation of Flexoelectric Coefficients of a MoS<sub>2</sub> monolayer with a**  
2 **Model of Self-consistently Distributed Effective Charges and Dipoles**

3 Yida Yang, Laurent Hirsinger, and Michel Devel<sup>a)</sup>  
4 *FEMTO-ST institute, UBFC, CNRS, ENSMM, 15B*  
5 *avenue des Montboucons, 25030 Besançon CEDEX,*  
6 *France*

Flexoelectricity is an electromechanical coupling phenomenon, that can generate noticeable electric polarization in dielectric materials for nanoscale strain gradients. It is gaining an increasing attention because of its potential applications, and the fact that experimental results were initially an order of magnitude higher than initial theoretical predictions. This stimulated intense experimental and theoretical researches to investigate flexoelectric coefficients in dielectric materials such as two-dimensional materials. In this work, we concentrate on the calculation of the flexoelectric coefficients of 2D-MoS<sub>2</sub> thanks to a model using self-consistently determined charges and dipoles on the atoms. More specifically, we study the importance of two contributions which were neglected/omitted in previous papers using this model, namely the charge term in the total polarization and the conservation of electric charge through a Lagrange multiplier. Our calculations demonstrate that the results for flexoelectric coefficients computed with this improved definition of polarization agree better with experimental measurements, provided consistent definitions for signs are used. Additionally, we show how two physical contributions with opposite signs compete to give net values of flexoelectric coefficients that can be either positive **or** negative depending on their relative importance, and give net values for the case of MoS<sub>2</sub>.

---

<sup>a)</sup>Electronic mail: michel.devel@femto-st.fr

## 7 I. INTRODUCTION

8 Flexoelectricity<sup>1</sup>, a fascinating electromechanical phenomenon, is widely em-  
9 ployed to describe electric polarization caused by strain gradient. Unlike piezo-  
10 electricity, which arises only in noncentrosymmetric materials, flexoelectricity can  
11 a priori exist in all materials. Therefore, flexoelectricity can provide new oppor-  
12 tunities to use some centrosymmetric materials to build electromechanical sys-  
13 tems, such as energy harvesters<sup>2,3</sup>, actuators<sup>4,5</sup>, flexible electronics<sup>6</sup>, flexoelectric  
14 sensors<sup>7,8</sup>.

15 Flexoelectricity was first predicted by Mashkevich and Tolpygo<sup>9</sup> during Tolpygo's  
16 studies on the optical and elastic properties of crystals. The polarization due to  
17 the flexoelectric effect was later phenomenologically described by Kogan<sup>10</sup>, using  
18 the contraction of a fourth order flexoelectricity tensor with the third order strain  
19 gradient tensor. Ever since the terminology 'flexoelectricity' was firstly borrowed  
20 from the liquid crystals community by Indenbom<sup>11,12</sup> et al in 1981, a great deal  
21 of theoretical work has been done to advance the development of the theory of  
22 flexoelectricity in solids. Earlier theoretical descriptions principally concentrated  
23 on lattice dynamics using Kogan's phenomenological theory<sup>10,13,14</sup> and continuum  
24 mechanics<sup>15</sup> or microscopic theories based on lattice dynamics<sup>13,16-18</sup> and quantum  
25 mechanics<sup>19-22</sup>. Calculations used methods such as core-shell model<sup>17,23</sup>, rigid-ion  
26 model<sup>13,14</sup>, molecular dynamics simulations<sup>24-26</sup>, finite element method<sup>27,28</sup> and  
27 phase-field method<sup>29</sup>. Recently, the advancement and popularity of machine  
28 learning techniques<sup>30-32</sup> provide original means for the computation of flexoelec-  
29 tricity coefficients. **Another strategy combining isogeometric analysis (IGA) and**  
30 **the Method of Moving Asymptotes (MMA) allows to extract both the real and**  
31 **complex parts of the piezoelectric and flexoelectric coefficients from electrical**  
32 **impedance curves<sup>34</sup>. This complements another technique based on topology op-**  
33 **timization methods to design multi-material flexoelectric structures, using the**  
34 **electromechanical coupling coefficient as figure of merit<sup>33</sup>.**

35 Flexoelectricity in solids was believed to be a very small effect. However, at  
36 the beginning of the 2000s, Ma and Cross reported unexpectedly high experimen-  
37 tal flexoelectric responses in a variety of perovskite ceramics<sup>35–40</sup> greatly arousing  
38 the interest in research of flexoelectricity in perovskite ceramics.<sup>41–43</sup> Furthermore,  
39 the relative importance of the flexoelectric effect with respect to the piezoelectric  
40 effect should increase as the scale of strain inhomogeneities decreases. Therefore,  
41 the recent development of ultrathin (2D) nanomaterials, due to the desired need  
42 for miniaturized devices, provide opportunities for researchers to study flexoelec-  
43 tricity in 2D materials which could offer interesting electromechanical coupling  
44 in nanodevices. Such an interest has stimulated intense research to investigate  
45 flexoelectric coefficients in carbon nanomaterials<sup>20,21,44–46</sup> (nanotubes, fullerenes,  
46 nanocores and patterned graphene), phosphorene<sup>47</sup>, hexagonal boron nitride<sup>48</sup> and  
47 transition-metal dichalcogenides<sup>49,50</sup> by means of first-principle calculations. Re-  
48 markably, Kumar et al very recently calculated the flexoelectric coefficient for  
49 fifty-four representative atomic monolayers selected from distinct groups in the  
50 periodic table of elements using ab-initio Density Functional Theory (DFT)<sup>51</sup>.

51 Recently, Zhuang and co-workers used molecular dynamics simulations cou-  
52 pled with a charge dipole (QP) model to compute flexoelectric coefficients for  
53 transition-metal dichalcogenides<sup>52</sup> and related materials<sup>53</sup>. This kind of method  
54 uses calculations much faster than DFT calculations, and provides an easier way  
55 to predict the properties of bigger and less symmetric heterostructures. Since we  
56 have some experience in using the QP model<sup>54–56</sup> we studied those papers in de-  
57 tails and noticed that a term involving effective charges was neglected/omitted in  
58 the definition of polarization that only used the effective dipoles, as in the case of  
59 covalent materials such as e.g. graphene. Furthermore, the enforcement of charge  
60 conservation was also not implemented, meaning that charges could flow in or  
61 out of the materials without any constraint, which can conflict with the fact that  
62 an insulating substrate (Polydimethylsiloxane (PDMS), Au, Al<sub>2</sub>O<sub>3</sub>)<sup>57,58</sup> was used

63 to obtain the out-of-plane effective flexoelectricity coefficient of monolayer MoS<sub>2</sub>,  
64 by using an equation for converse flexoelectricity to link the out-of-plane effective  
65 piezoelectric coefficient measured by piezoresponse force microscopy and the flexo-  
66 electric coefficient to be determined<sup>57,58</sup>. We also note that in-plane flexoelectric  
67 coefficients  $\mu_{1111}$  or  $\mu_{2222}$  for such 2D materials have not yet been experimentally  
68 obtained, since it has been difficult to isolate the relative contributions of piezo-  
69 electricity and flexoelectricity to the resulting polarization.

70 In this work, we computed the in-plane flexoelectric coefficients  $\mu_{1111}$ ,  $\mu_{2222}$ ,  
71 transverse flexoelectric coefficient  $\mu_{3311}$  and out-of-plane flexoelectric coefficient  
72  $\mu_{3333}$  for monolayer MoS<sub>2</sub> using the charge-dipole model<sup>59</sup> with radial Gaussian  
73 regularization<sup>54,56,60-63</sup> enforcing charge conservation with a Lagrange multiplier  
74 and adding an ionic charge term in the definition of polarization. The significance  
75 of the missing charge term is estimated in the computation of  $\mu_{3333}$ , by compar-  
76 ison with the simulation paper of Javvaji et al.<sup>53</sup> and the experimental papers  
77 of Brennan et al.<sup>57,58</sup>. Our calculations illustrate that the results for this flexo-  
78 electric coefficient computed with the improved definition of polarization agree in  
79 magnitude with experimental measurements, with the possible reason causing the  
80 discrepancy in sign discussed. Moreover, two critical factors capable of affecting  
81 the sign of flexoelectric coefficient are fully elucidated while  $\mu_{3311}$  is computed.  
82 Additionally,  $\mu_{1111}$  and  $\mu_{2222}$  are calculated by using an in-plane displacement field  
83 that effectively eliminates the piezoelectric contribution to the polarization.

84 This paper is organized as follows. In Sec.II we describe the Gaussian reg-  
85 ularized charge-dipole model, our bending simulation set-ups and the computa-  
86 tional methodology for the computation of the strain gradient. The computation  
87 of in-plane flexoelectric coefficient  $\mu_{1111}$ ,  $\mu_{2222}$ , transverse flexoelectric coefficient  
88  $\mu_{3311}$  and out-of-plane flexoelectric coefficient  $\mu_{3333}$  are presented and discussed in  
89 Sec.III. Section IV concludes our findings.

## 90 II. METHODS

### 91 A. Principle of the method used to compute flexoelectricity

#### 92 coefficients

As written in the introduction, the direct flexoelectric effect describes the fact that a strain gradient in a material will cause an (additional) electric polarization of the material, because of the inhomogeneous distribution of positive and negative charge centers caused by the inhomogeneous deformation. Polarization being a vector described by a vector (first order tensor) and strain gradient a third order tensor, the supposedly linear relation between these two quantities is represented by a fourth order flexoelectricity tensor. Various conventions for the signification of the indices, leading to different matrix compressed representations, are used in the literature. We chose the one that puts the index corresponding to the polarization in first place, since we do not make use of the equivalence of the two strain indices:

$$\Delta P_i = \mu_{ijkl} G_{jkl} \quad (1)$$

93 where  $i, j, k, l$  are indices labeling the coordinates  $x, y, z$  or  $1, 2, 3$ . The Einstein  
94 implied summation convention for repeated indices is used.

95 Our goal is to compute values for these  $\mu_{ijkl}$  coefficients. For that purpose we  
96 will use an inverse effect: when submitted to an external electric field, a dielectric  
97 material tends to deform so as to align its global dielectric polarization vector with  
98 the external field. Hence, we use various symmetric field configurations designed  
99 to deform inhomogeneously a MoS<sub>2</sub> monolayer, while not changing the global po-  
100 larization contributions due to the dielectric susceptibility of the material or its  
101 piezoelectric properties. Then, we compute both the global polarization and the  
102 global strain gradient of the deformed structure and fit the (hopefully linear) re-  
103 lation between these two quantities to find the  $\mu$  coefficients.

104 We shall therefore describe now, how we compute the global polarization and

105 strain gradient in the monolayer.

106 **B. Description of the charge dipole model used to compute the**  
 107 **polarization of a monolayer MoS<sub>2</sub> subjected to an external electric field**

We start with the regularized charge-dipole (QP) model<sup>54,56,60–63</sup>, in which each atom of a MoS<sub>2</sub> nanoribbon is described by the combination of an effective charge and a dipole with radial Gaussian distributions, plus an effective electronegativity. The total electrostatic energy  $E_{elec}$  associated with those effective charges  $\{q_\alpha\}$  and dipoles  $\{\mathbf{p}_\alpha\}$  located at the atomic positions  $\{\mathbf{r}_\alpha\}$  (with  $\alpha = 1, \dots, N$ ), in the presence of an external electric field  $\mathbf{E}_{ext}$  is given by:

$$E_{elec} = \sum_{\alpha=1}^N q_\alpha(\chi_\alpha + V_{ext,\alpha}) - \sum_{\alpha=1}^N \mathbf{p}_\alpha \cdot \mathbf{E}_{ext} + \frac{1}{2} \sum_{\alpha=1}^N \sum_{\beta=1}^N q_\alpha T_{q-q}^{\alpha,\beta} q_\beta - \sum_{\alpha=1}^N \sum_{\beta=1}^N \mathbf{p}_\alpha \cdot \mathbf{T}_{p-q}^{\alpha,\beta} q_\beta - \frac{1}{2} \sum_{\alpha=1}^N \sum_{\beta=1}^N \mathbf{p}_\alpha \cdot \mathbf{T}_{p-p}^{\alpha,\beta} \cdot \mathbf{p}_\beta \quad (2)$$

where  $N$  stands for the number of atoms in the structure considered and  $\chi_\alpha$  is the electronegativity of the atom  $\alpha$ , once inserted in the molecule.  $V_{ext,\alpha}$  is the electrostatic potential at  $\mathbf{r}_\alpha$  corresponding to the external electric field, which can be expressed as  $-\mathbf{E}_{ext} \cdot \mathbf{r}_\alpha$  in the case of a uniform external field.  $T_{q-q}$ ,  $\mathbf{T}_{p-q}$  and  $\mathbf{T}_{p-p}$  are interaction tensors between effective point charges or dipoles in vacuum (see equation 3), which have been convoluted with one radial Gaussian distribution per atom, of the form  $\pi^{3/2} R_\alpha^3 \exp(-|\mathbf{r} - \mathbf{r}_\alpha|^2 / R_\alpha^2)$ . This allows to take into account approximately the extension of the electronic clouds, and prevents the occurrence of divergence problems, i.e. polarization catastrophes, that can occur in simulations when two atoms are so close to each other that the approximation of an interaction between point charges or dipoles is not a good approximation

any more.<sup>60-62,64,65</sup>

$$\left\{ \begin{array}{l} T_{q-q}^{\alpha\beta} = \frac{1}{4\pi\epsilon_0 r_{\alpha\beta}} \operatorname{erf}\left(\frac{r_{\alpha\beta}}{\sqrt{R_\alpha^2 + R_\beta^2}}\right) \\ \mathbf{T}_{p-q}^{\alpha\beta} = -\nabla_{\mathbf{r}_\alpha} T_{q-q}^{\alpha\beta} = -\frac{1}{4\pi\epsilon_0} \frac{r_{\alpha\beta}}{r_{\alpha\beta}^3} \left[ \operatorname{erf}\left(\frac{r_{\alpha\beta}}{\sqrt{R_\alpha^2 + R_\beta^2}}\right) - \frac{2}{\sqrt{\pi}} \frac{r_{\alpha,\beta}}{\sqrt{R_\alpha^2 + R_\beta^2}} \exp\left(-\frac{r_{\alpha\beta}^2}{R_\alpha^2 + R_\beta^2}\right) \right] \\ \mathbf{T}_{p-p}^{\alpha\beta} = -\nabla_{\mathbf{r}_\beta} \otimes \nabla_{\mathbf{r}_\alpha} T_{q-q}^{\alpha\beta} \\ = \frac{1}{4\pi\epsilon_0} \left\{ \frac{3\mathbf{r}_{\alpha\beta} \otimes \mathbf{r}_{\alpha\beta} - r_{\alpha\beta}^2 \mathbf{I}}{r_{\alpha\beta}^5} \left[ \operatorname{erf}\left(\frac{r_{\alpha\beta}}{\sqrt{R_\alpha^2 + R_\beta^2}}\right) - \frac{2}{\sqrt{\pi}} \frac{r_{\alpha,\beta}}{\sqrt{R_\alpha^2 + R_\beta^2}} \exp\left(-\frac{r_{\alpha\beta}^2}{R_\alpha^2 + R_\beta^2}\right) \right] \right. \\ \left. - \frac{4}{\sqrt{\pi}} \frac{\mathbf{r}_{\alpha\beta} \otimes \mathbf{r}_{\alpha\beta}}{r_{\alpha\beta}^2} \frac{1}{(\sqrt{R_\alpha^2 + R_\beta^2})^3} \exp\left(-\frac{r_{\alpha\beta}^2}{R_\alpha^2 + R_\beta^2}\right) \right\} \end{array} \right. \quad \forall \alpha \neq \beta \quad (3)$$

where  $\mathbf{r}_{\alpha\beta} = \mathbf{r}_\beta - \mathbf{r}_\alpha$  is the vector pointing from  $\alpha^{th}$  atom to  $\beta^{th}$  atom.  $R_\alpha$  and  $R_\beta$  are the characteristic widths of Gaussian charge distributions for atom type  $\alpha$  and  $\beta$  respectively. In the limit  $\mathbf{r}_\alpha = \mathbf{r}_\beta$ , the expressions of the various  $T^{\alpha,\beta}$  interaction tensors in equation 3 converge to finite values (Eq. 4) related to the self-energy for each atom (atomic 'capacitance' or chemical hardness and polarizability).

$$\left\{ \begin{array}{l} q_\alpha T_{q-q}^{\alpha,\alpha} q_\alpha = \frac{q_\alpha^2}{4\pi\epsilon_0} \frac{\sqrt{2/\pi}}{R_\alpha} \\ \mathbf{p}_\alpha \cdot \mathbf{T}_{p-q}^{\alpha,\alpha} q_\alpha = 0 \\ \mathbf{p}_\alpha \cdot \mathbf{T}_{p-p}^{\alpha,\alpha} \cdot \mathbf{p}_\alpha = -\frac{p_\alpha^2}{4\pi\epsilon_0} \frac{\sqrt{2/\pi}}{3R_\alpha^3}. \end{array} \right. \quad (4)$$

108 Our version of the QP model for MoS<sub>2</sub> possesses 8 parameters: 2 ( $\chi$  and  $R$ )  
109 per kind of atoms by 4 kinds: Mo and S 'bulk' + Mo and S 'edge'. Details on  
110 this parameterization, by comparison with DFT data, are given in our previous  
111 work.<sup>56</sup>

The charges and dipoles at electrostatic equilibrium are then determined by minimizing the electrostatic energy (Eq. 2) using a Lagrange multiplier  $\lambda$  to enforce charge conservation in the nanoribbon:

$$f = E_{elec} + \lambda \left( \sum_{\alpha=1}^N q_\alpha - Q_{tot} \right) \quad (5)$$

112 This Lagrange multiplier can be physically interpreted as the chemical potential  
113 of the molecule.<sup>61</sup> This enforcement of charge conservation within the framework



114 of QP model is quite essential since it ensures that charges stay in the material  
 115 in order to mimic the conditions of experimental measurements.<sup>58</sup> Requiring the  
 116 derivative of function  $f(q, \mathbf{p}, \lambda)$  with respect to  $q_\alpha, p_{x,\alpha}, p_{y,\alpha}, p_{z,\alpha}$  and  $\lambda$  to be zero  
 117 will give a system of  $4N + 1$  linear equations for determining the  $4N + 1$  scalar  
 118 unknowns ( $q_\alpha, p_{x,\alpha}, p_{y,\alpha}, p_{z,\alpha}$  and  $\lambda$ ). These linear equations may be written in a  
 119 matrix form:

$$\begin{bmatrix} T_{q-q} & \mathbf{T}_{p-q}^t & 1 \\ \mathbf{T}_{p-q} & \mathbf{T}_{p-p} & 0 \\ 1 & 0 & 0 \end{bmatrix} \begin{bmatrix} q \\ \mathbf{p} \\ \lambda \end{bmatrix} = \begin{bmatrix} -(\chi + V_{ext}) \\ -\mathbf{E}_{ext} \\ Q_{tot} \end{bmatrix} \quad (6)$$

where  $T_{q-q}$  is a block matrix with  $N$  rows and  $N$  columns.  $\mathbf{T}_{p-p}$  is a block matrix with  $3N$  rows and  $3N$  columns.  $\mathbf{T}_{p-q}$  is a block matrix with  $3N$  rows and  $N$  columns.  $\mathbf{T}_{p-q}^t$  is the transpose of  $\mathbf{T}_{p-q}$ . Similarly, blocks  $q$  and  $-(\chi + V_{ext})$  have  $N$  rows and 1 column, while blocks  $\mathbf{p}$  and  $-\mathbf{E}_{ext}$  have  $3N$  rows and 1 column. We note that the solution can be written in two parts as:

$$\begin{bmatrix} q \\ \mathbf{p} \\ \lambda \end{bmatrix} = \begin{bmatrix} T_{q-q} & \mathbf{T}_{p-q}^t & 1 \\ \mathbf{T}_{p-q} & \mathbf{T}_{p-p} & 0 \\ 1 & 0 & 0 \end{bmatrix}^{-1} \begin{bmatrix} -\chi \\ 0 \\ Q_{tot} \end{bmatrix} + \begin{bmatrix} T_{q-q} & \mathbf{T}_{p-q}^t & 1 \\ \mathbf{T}_{p-q} & \mathbf{T}_{p-p} & 0 \\ 1 & 0 & 0 \end{bmatrix}^{-1} \begin{bmatrix} -V_{ext} \\ -\mathbf{E}_{ext} \\ 0 \end{bmatrix} \quad (7)$$

where the first term on the right side corresponds to intrinsic charges  $q_\alpha^0$  and dipoles  $\mathbf{p}_\alpha^0$ , i.e. charges and dipoles in the absence of any external electric field, that can however vary due to a mechanical deformation. The electronegativities  $\chi_\alpha$  uniquely determine these intrinsic charges and dipoles (given the atomic positions), independently from any external electric field  $\mathbf{E}_{ext}$  or potential  $V_{ext}$ . For our calculations, the total charge of the nanoribbon ( $Q_{tot}$ ) is set to be zero because of the fact that flexoelectricity is supposed to be an intrinsic property, therefore requiring no extra charge to appear. The second term on the right side corresponds to effective additional charges ( $q_\alpha^{ind}$ ) and dipoles ( $p_\alpha^{ind}$ ) generated by the external

electric field and potential). This can be summarized under the form:

$$\left\{ \begin{array}{l} p_x = \sum_{\alpha=1}^N (p_{x,\alpha}^0 + p_{x,\alpha}^{ind}) \\ p_y = \sum_{\alpha=1}^N (p_{y,\alpha}^0 + p_{y,\alpha}^{ind}) \\ p_z = \sum_{\alpha=1}^N (p_{z,\alpha}^0 + p_{z,\alpha}^{ind}) \\ q = \sum_{\alpha=1}^N (q_{\alpha}^0 + q_{\alpha}^{ind}) \end{array} \right. \quad (8)$$

In terms of the calculated dipoles  $\mathbf{p}$  and charges  $q$ , the global polarization  $\mathbf{P}$  for MoS<sub>2</sub> nanoribbon is defined as<sup>59</sup>:

$$\mathbf{P} = \frac{\sum_{\alpha=1}^N (q_{\alpha} \mathbf{r}_{\alpha} + \mathbf{p}_{\alpha})}{V} \quad (9)$$

120 in which  $V$  is the volume of MoS<sub>2</sub> nanoribbon. A thickness of 6.5 Å is used in  
 121 computing  $V$ .<sup>66</sup> More information on the charge dipole model for MoS<sub>2</sub> can be  
 122 found in our previous work<sup>56</sup>. Note that since MoS<sub>2</sub> is not ferroelectric, the total  
 123 contribution to polarization of the  $q_{\alpha}^0$  and  $\mathbf{p}_{\alpha}^0$  is zero (verified numerically), so that  
 124 Eq. 9 could be rewritten by taking into account the induced charges and dipoles  
 125 only.

126 In order to compare with some DFT results or remove edge effects, periodic  
 127 boundary conditions can be applied in the QP model by adding the contributions  
 128 of periodic images in the interaction tensors, i.e. adding contributions obtained by  
 129 replacing  $r_{\alpha\beta}$  in Eq.3 with  $r_{\alpha\beta} + L * p$  ( $p \in [-k, k]$ ), with  $L$  denoting the periodic  
 130 length in a given direction and  $k$  being a very large integer. We verified that  
 131 setting  $k = 100$  in our calculation is already sufficiently large to reach convergence  
 132 in the computation of in-plane flexoelectric coefficients  $\mu_{1111}$ ,  $\mu_{2222}$  and out-of-plane  
 133 flexoelectric coefficient  $\mu_{3333}$ , thus eliminating edge effects.

## 134 C. Calculation of flexoelectricity coefficients

135 We illustrate the method we use to compute the flexoelectric coefficients on the  
136 special case of the determination of  $\mu_{3311}$ .

### 137 1. *potential energy functional used for the 'structure' part*

138 The key of the molecular simulations is actually the interatomic potential, which  
139 is applied to describe the interaction among atoms. For single-layer MoS<sub>2</sub>, the  
140 Stillinger-Weber many-body potential ( $E_{SW}$ ) as parameterized by Wen et al<sup>67</sup> was  
141 very recently proven to be robust through a quantitative systematic comparison of  
142 structural and mechanical properties, as well as phonon dispersion for single-layer  
143 MoS<sub>2</sub> using density functional theory (DFT) and molecular statics calculations.<sup>68</sup>  
144 We therefore used this parameterization of the SW potential ( $E_{SW}$ ) in our simula-  
145 tions, and found it very stable. Its analytical form and the values of the parameters  
146 are recalled in [Supplementary material](#). The various MoS<sub>2</sub> nanoribbons we use in  
147 our simulations are thus initially relaxed by minimizing  $E_{SW}$ . This gives the un-  
148 deformed configuration mentioned in the previous subsection.

149 To compute the deformed configurations, we removed the interactions between  
150 intrinsic charges and dipoles in  $E_{elec}$ , since they are already included in  $E_{SW}$ .  
151 We also neglected the total contribution of the interactions between intrinsic and  
152 induced charges and dipoles to keep only the total contributions of the interactions  
153 between charges and dipoles induced by the external field and potential (which we  
154 name  $E'_{elec}$ ).

### 155 2. *Initial conditions for the calculation of $\mu_{3311}$*

156 In order to compute  $\mu_{3311}$ , a  $\searrow/\swarrow$ -like external electric field  $\mathbf{E}_{ext}$ , with both  
157 directions of  $\mathbf{E}_{ext}$  in the  $x$ - $z$  plane, is applied to the MoS<sub>2</sub> nanoribbon, keeping the

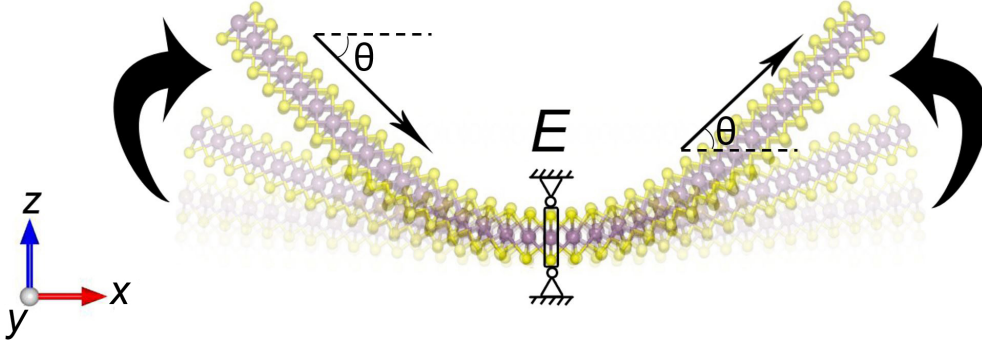


FIG. 1. Schematic of bending simulation for MoS<sub>2</sub> nanoribbon subjected to an external electric field. The left and right parts of the MoS<sub>2</sub> sheet are submitted to an electric field in the bottom-right and top-right direction, respectively. The external electric field  $\mathbf{E}$  is represented by the arrows.  $\theta$  is the angle with the  $+x$  direction.

158 middle row of atoms fixed (as if it were attached to a virtual fixed object). This  
 159 field generates a bending deformation of the nanoribbon because of the inverse  
 160 flexoelectric effect, as seen in Fig 1. The conjugate gradient algorithm is then  
 161 used to minimize the energy function  $E_{tot} = E_{SW} + E'_{elec}$  which now includes  
 162 the interactions with the external field and potential and the contributions of the  
 163 effective induced charges and dipoles. The energy optimization simulation then  
 164 makes the MoS<sub>2</sub> flake bend towards the direction of the applied electric field by  
 165 adjusting the positions of the atoms until the computed average force is less than  
 166 0.00004 eV/Å. Note that all these simulations are done with a FORTRAN code  
 167 that has been continuously developed in the group for years.

168 The mechanism of electrostatic bending of MoS<sub>2</sub> flake is depicted in Figure  
 169 1 of Supplementary material. We can see that negative and positive charges are  
 170 shifted to opposite directions due to the non-zero transversal electric field (positive  
 171 charges move to upper left and negative ones move to top right of the MoS<sub>2</sub> flake).  
 172 The interaction between the electric field generated by the induced charges and  
 173 the external electric field produces two torques with opposite direction, termed  $\tau_1$

174 and  $\tau_2$ , which may be expressed as  $q\mathbf{r} \times \mathbf{E}_{ext}$ , making the two sides of the MoS<sub>2</sub>  
 175 flake respectively bend towards the direction of the external electric field with the  
 176 fixed atoms as the rotation axis, while giving a zero total polarization along the  
 177 vertical axis.

### 178 3. Calculation of $\mu_{3311}$

Contributions to the polarization of a given dielectric material submitted to an external electric field may come from piezoelectricity, flexoelectricity and electric susceptibility. In the simulations defined in the previous subsection, piezoelectricity may not be taken into account due to the symmetric bending deformation<sup>52</sup>. This makes the total induced polarization due to the first order deformation gradient become zero. Additionally, one can find the total external electric field along the out-of-plane is also zero. Hence, the out-of-plane polarization equal to the product of the susceptibility and the electric field should be removed as well. The remaining flexoelectric part of the out-of-plane polarization  $P_3$  can be written as:

$$P_3 = \sum_{j=1}^3 \sum_{k=1}^3 \sum_{l=1}^3 \mu_{3jkl} G_{jkl} \quad (10)$$

with  $\mu_{3jkl}$  standing for flexoelectric tensor components. With the setup defined in the previous section, this can be approximated by:

$$P_3 = \mu_{3311} G_{311} \quad (11)$$

179 Hence  $\mu_{3311}$  can be determined as the slope of the supposedly linear relation be-  
 180 tween  $P_3$  and  $G_{311}$ . Details on the computing method for determining strain  
 181 gradient can be found in Supplementary material.

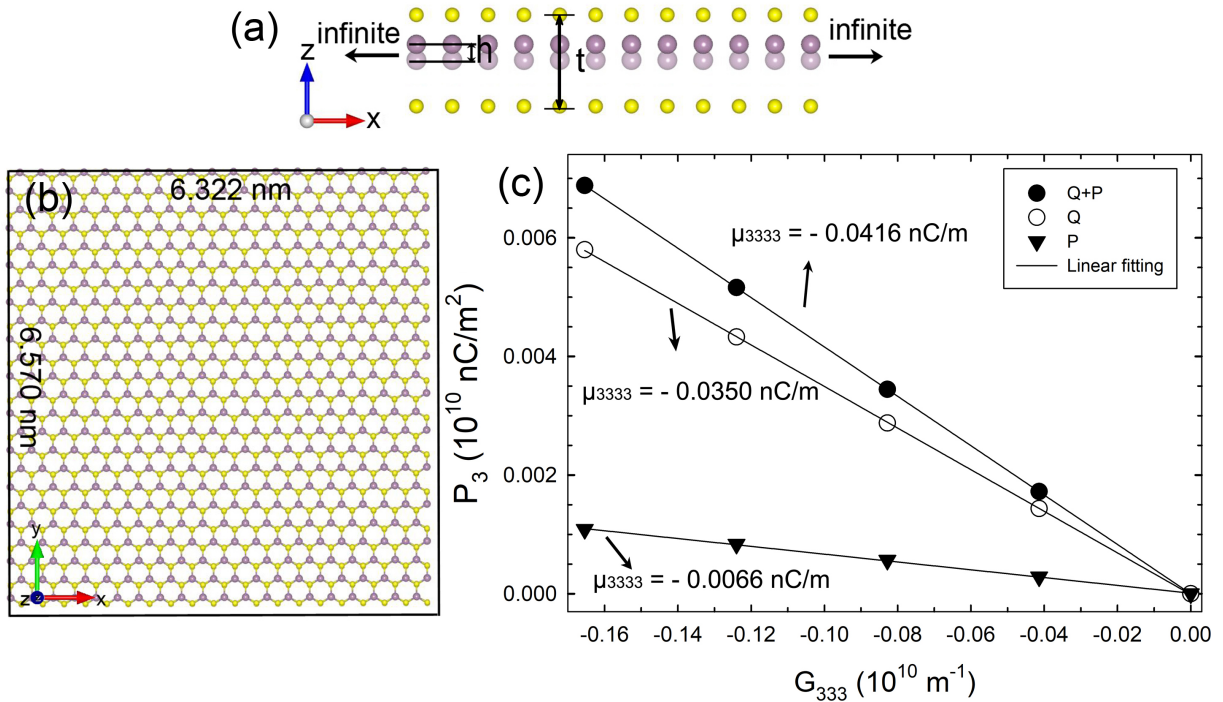


FIG. 2. (a) Schematic diagram of creation of strain gradient  $G_{333}$  inside monolayer MoS<sub>2</sub>.  $h$  and  $t$  stand for the small upward shift for a layer of molybdenum atom and the geometric thickness of monolayer MoS<sub>2</sub>, respectively. (b) Basic unit for periodic monolayer MoS<sub>2</sub>, with length and width of basic unit being 6.570 nm and 6.322 nm, respectively. (c) Variation of polarization  $P_3$  with strain gradient  $G_{333}$  for monolayer MoS<sub>2</sub>.

### 182 III. RESULTS AND DISCUSSION

183 In this section, we discuss the results we got for the computation of the in-  
 184 plane flexoelectric coefficients  $\mu_{1111}$ ,  $\mu_{2222}$ , the transverse flexoelectric coefficient  
 185  $\mu_{3311}$  and the out-of-plane coefficient  $\mu_{3333}$ . The parameters for  $E_{SW}$  and QP  
 186 model used in this work were initially validated through calculation of the in-  
 187 plane piezoelectric constant  $e_{222}$  for an MoS<sub>2</sub> monolayer. We found a value of the  
 188 same order of magnitude as the corresponding experimental result (more details

189 are given in Supplementary material).

## 190 A. Out-of-plane flexoelectric coefficient $\mu_{3333}$

191 As can be seen on Fig.2a, for this calculation, the layer of molybdenum atoms  
192 is shifted a small distance  $h$  to the positive direction of  $z$  axis to generate a strain  
193 gradient only along the out-of-plane ( $z$ ) direction. In this case, the unique strain  
194 gradient that does exist is  $G_{333}$  and the expression for computing  $\mu_{3333}$  can be  
195 written as  $\mu_{3333} = \frac{\partial P_3}{\partial G_{333}}$ . The geometric thickness of monolayer MoS<sub>2</sub> is  $t$ . With  
196 both  $h$  and  $t$ , the strain gradient  $G_{333}$  can be computed as  $-\frac{8h}{t^2}$ , which may be  
197 derived by:  $G_{333} = \frac{d^2 u_z(0)}{dz^2} \approx \frac{u_z(-\frac{t}{2}) + u_z(\frac{t}{2}) - 2u_z(0)}{(t/2)^2} = \frac{0+0-2h}{(t/2)^2} = -\frac{8h}{t^2}$ , with  $u_z(\frac{t}{2})$ ,  
198  $u_z(-\frac{t}{2})$  and  $u_z(0)$  representing the displacement of atoms for top sulfur layer,  
199 bottom sulfur layer and molybdenum layer, respectively. In this calculation, we  
200 enforce periodic boundary conditions to eliminate edge effects that can be quite  
201 important in such a setup. As can be seen on Fig.2b, we use a MoS<sub>2</sub> flake with a  
202 width of 6.164 nm and a length of 6.388 nm as supercell, which gives periods along  
203  $x$  and  $y$  direction of 6.322 nm and 6.570 nm, respectively. Bond length between  
204 Mo and S is set as 2.39763 Å in the presence of periodic boundary conditions.  
205 On Fig.2c, we plot the polarization  $P_3$  as a function of  $G_{333}$ , in order to obtain  
206 the flexoelectric coefficient  $\mu_{3333}$  of 2D MoS<sub>2</sub>. Three different ways to compute  
207 the polarization are used (using  $q_\alpha \mathbf{r}_\alpha$  only, using  $\mathbf{p}_\alpha$  only or using both terms in  
208 Eq.9, with charges and dipoles computed using the QP scheme in the three cases).  
209 The units of polarization  $P_3$  and strain gradient  $G_{333}$  are converted from  $e/\text{Å}^2$   
210 and  $\text{Å}^{-1}$  to  $10^{10}$  nC/m<sup>2</sup> and  $10^{10}$  m<sup>-1</sup> respectively, so as to readily obtain  $\mu_{3333}$  in  
211 nC/m from the slope of the fitted straight line. We compare  $\mu_{3333}$  computed under  
212 the various definitions of polarization with that obtained from the experimental  
213 measurements conducted by Brennan et al in 2017 and 2020<sup>57,58</sup>, respectively, as  
214 shown in Table I.

TABLE I. Comparison between out-of-plane flexoelectric coefficients  $\mu_{3333}$  obtained by charge-dipole model and experimental measurements. The two different contributions to the polarization coming from charges alone or dipoles alone are considered separately then together for the computation of  $\mu_{3333}$  by the charge-dipole model.

| Ref.                               | $\mu_{3333}$ (nC/m) | Definition of polarization   |
|------------------------------------|---------------------|--|
| present work                       | -0.0416             | $P_3 = \frac{\sum_{\alpha=1}^N (q_{\alpha} r_{3,\alpha} + p_{3,\alpha})}{V}$ |
| present work                       | -0.0350             | $P_3 = \frac{\sum_{\alpha=1}^N q_{\alpha} r_{3,\alpha}}{V}$                  |
| present work                       | -0.0066             | $P_3 = \frac{\sum_{\alpha=1}^N p_{3,\alpha}}{V}$                             |
| Brennan et al (2017) <sup>57</sup> | 0.08 or 0.12        | ————   |
| Brennan et al (2020) <sup>58</sup> | 0.065               | ————   |

215 It can be seen that the result for  $\mu_{3333}$  computed when the charge term is  
216 included in the definition of polarization will be comparatively closer to the exper-  
217 imental result in absolute value whereas  $\mu_{3333}$  computed with the dipole term only  
218 considered is of the same order of magnitude but much smaller than the experi-  
219 mental value. This manifests that the charge term, omitted/neglected in Ref.<sup>52</sup>,  
220 cannot be neglected for the calculation of polarization for MoS<sub>2</sub>. We do not take  
221 into account the discrepancy in sign between our computed results and the results  
222 of the Piezoresponse Force Microscopy (PFM) measurements of Brennan et al.,  
223 since we believe that it is due to a problem of different definition for the algebraic  
224 (or not) radius of curvature. This is reflected in another experimental measure-  
225 ments of out-of-plane flexoelectric coefficient  $\mu_{3333}$  for few-layers MoS<sub>2</sub> with PFM,  
226 very recently conducted by Hirakata et al<sup>69</sup>. In their work, the sign of the out-  
227 of-plane flexoelectric coefficient is measured to be negative, though they quote a  
228 positive number. Indeed, using their Eq. 9, one can get  $\mu_{3333} = \mu_{39} = -c_{33}\epsilon_3/\frac{\partial E_3}{\partial x_3}$ .



229 Since  $c_{33}$ ,  $\epsilon_3$  and  $\frac{\partial E_3}{\partial x_3}$  (see their Figure 11) are all positive, their  $\mu_{3333}$  is in fact  
230 negative.<sup>69</sup>

231 Other problems could arise because the MoS<sub>2</sub> samples used in the PFM exper-  
232 iments might not be as perfect as that used in our calculation. Indeed, intrinsic  
233 atomic defects have been observed in the CVD-grown monolayer MoS<sub>2</sub> using near-  
234 field photoluminescence imaging<sup>70</sup>. These defects could give rise to very localized  
235 strain gradients and therefore to noticeable additional polarization due to flexo-  
236 electricity, since monolayer MoS<sub>2</sub> is sensitive to any tiny deformation along vertical  
237 direction ( $z$ ) due to its atomically thin thickness. Furthermore, the possibly exist-  
238 ing interfacial contamination between substrate and MoS<sub>2</sub> sample and the other  
239 uncertainties relevant to the measurements could be another cause of discrepancy  
240 between our theoretical results and the experimental ones. It would be useful if  
241 these (difficult) experiments could be repeated many times, so as to reduce the  
242 large uncertainties on the experimental results, but we feel that our present results  
243 for  $\mu_{3333}$  of a MoS<sub>2</sub> monolayer, agree well enough with experiment, to encourage  
244 us to compute other flexoelectric coefficients for MoS<sub>2</sub> monolayer, for which we do  
245 not have experimental data to compare with.

## 246 B. Transverse flexoelectric coefficient $\mu_{3311}$

247 The bending simulation described in the 'Methods' section is employed to com-  
248 pute the transverse flexoelectric coefficient  $\mu_{3311}$  of MoS<sub>2</sub>. Since the visible dis-  
249 placements are mostly along  $z$  direction, the strain gradient enabling polarization  
250 to be nonzero is principally  $G_{311}$ . Hence,  $\mu_{3311}$  may be approximately expressed  
251 as  $\mu_{3311} = \frac{\partial P_3}{\partial G_{311}}$ . Fig.3a presents the variations of the out-of-plane polarization  $P_3$   
252 for a MoS<sub>2</sub> flake bent along ( $x$ ) zigzag direction with respect to the strain gradient  
253  $G_{311}$ . One can notice that the intercept of the linear-fitting straight line is almost  
254 zero, meaning that the nonzero polarization is mainly caused by  $G_{311}$ .

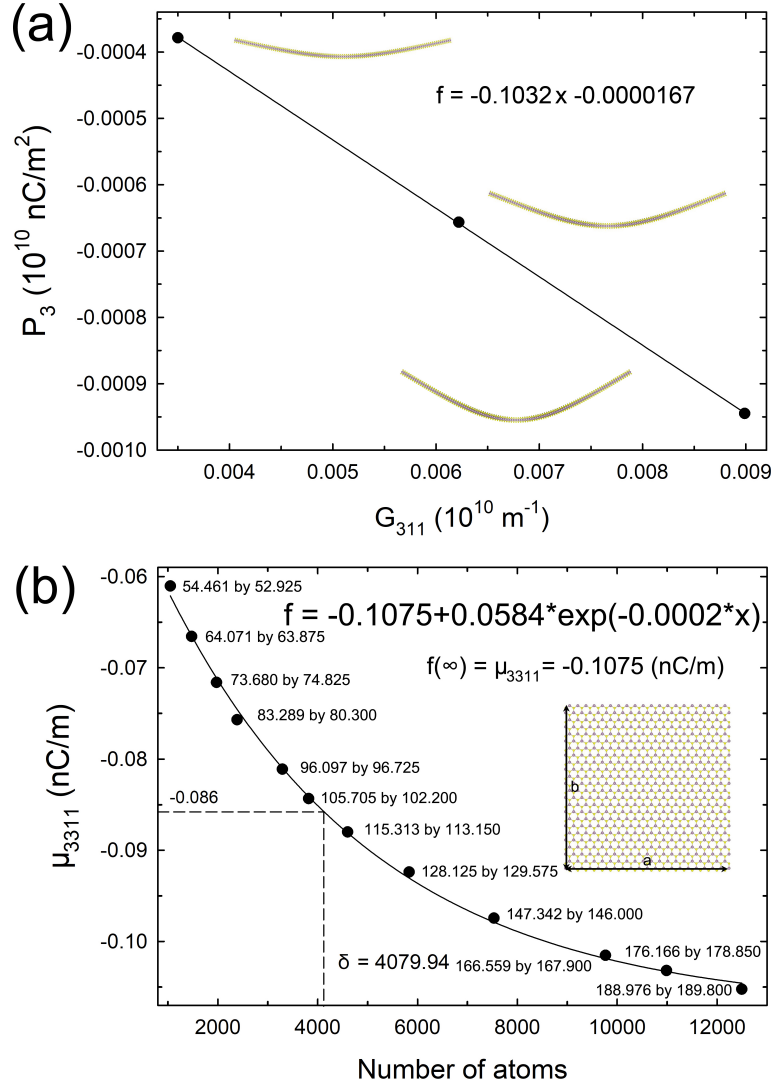


FIG. 3. (a) Variation of  $P_3$  with strain gradient  $G_{311}$ . The magnitude of the electric fields imposed to the MoS<sub>2</sub> monolayer for bending simulation are  $0.0424 \text{ V/\AA}$ ,  $0.0566 \text{ V/\AA}$ ,  $0.0707 \text{ V/\AA}$ , respectively. (b) Transverse flexoelectric coefficient  $\mu_{3311}$  vs number of atoms. An exponential function is used to describe the tendency to convergence. The lengths  $a$  and  $b$  of the sides the of MoS<sub>2</sub> flakes are marked next to each computed  $\mu_{3311}$ . The first and second number for the size of MoS<sub>2</sub> flake corresponds to  $a$  and  $b$ , respectively. The unit of  $a$  and  $b$  is  $\text{\AA}$ .  $\delta$  denotes characteristic length of exponential function. The angle between the electric field and the positive direction of the x-axis is set to 45 degrees.

255 Contrarily to what we did for the computation of  $\mu_{3333}$ , periodic boundary  
 256 conditions cannot be exerted in the bending simulation because bending of material  
 257 submitted to the external electric field will break the periodicity of the lattice itself.  
 258 We therefore studied the effect of the size of the MoS<sub>2</sub> flake, on the computed  
 259 flexoelectric coefficient. Fig.3b is plotted to present the variation of transverse  
 260 flexoelectric coefficient  $\mu_{3311}$  with the increasing number of atoms. It can be seen  
 261 that the value of  $\mu_{3311}$  scales non-linearly down with the number of atoms. The  
 262 larger the number of atoms, the more obvious the trend of curve convergence. To  
 263 obtain a converged value, data is fitted with an exponential function. With the  
 264 number of atoms increasing, the transverse flexoelectric coefficient  $\mu_{3311}$  converges  
 265 to  $-0.1075$  nC/m, comparable to that for phosphorene<sup>47</sup> and boron nitride sheet<sup>48</sup>.  
 266 A comparison is made between  $\mu_{3311}$  computed with QP model and that obtained  
 267 by DFT-based first principle calculation by Shashikant et al<sup>51</sup>, as listed in Table II.  
 268 It can be seen that our computed result for  $\mu_{3311}$  agrees much better in absolute  
 269 value with that obtained from DFT calculations than the one computed by Zhuang  
 270 et al.<sup>52</sup>, signifying that the computation of transverse flexoelectric coefficient of  
 271 MoS<sub>2</sub> can be well captured by the QP model, if the proper definition for the  
 272 polarization is used. **Note that the radial polarization  $\mathbf{p}_r$  defined in reference<sup>51</sup>**  
 273 **and<sup>71</sup> to compute  $\mu_{3311}$  can be considered equivalent to the  $p_z$  used in our work,**  
 274 **since it is always locally perpendicular to the 2D material.** We will now turn again  
 275 to the question of the sign of the flexoelectric coefficients.

277 Understanding the reason causing the discrepancy in the sign of flexoelectric  
 278 coefficients is essential because the direction of the electric polarization induced by  
 279 flexoelectricity is of significance for sensors and energy harvesters. We will study  
 280 successively the sign of the polarization and the strain gradient.

281 Concerning polarization, we separate two distinct contributions: one due to  
 282 the deformation of the lattice and the other one due to charge transfer between  
 283 the inner and outer layers during bending. For that purpose we first compute

TABLE II. Comparison between transverse flexoelectric coefficient  $\mu_{3311}$  obtained by charge dipole model and theoretical computation.

| Ref.                           | $\mu_{3311}$ (nC/m) |
|--------------------------------|---------------------|
| present work                   | -0.1075             |
| Shashikant et al <sup>51</sup> | 0.14                |
| Zhuang et al <sup>52</sup>     | 0.032               |

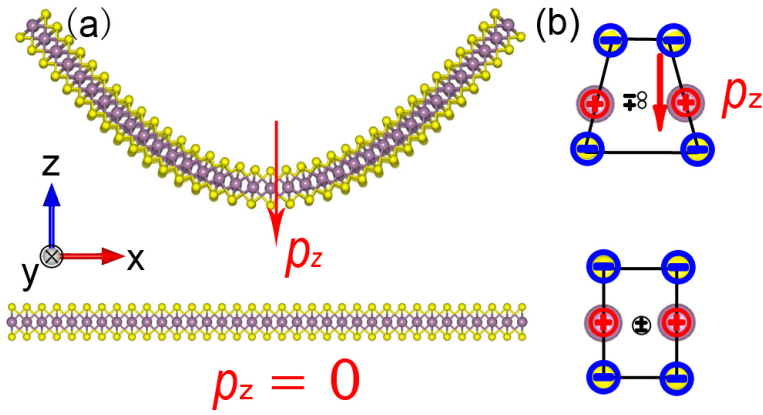


FIG. 4. Origin of flexoelectric effect in bending deformation. (a) Under bending deformation, the direction of induced dipole moment points to  $-z$  direction. For an undeformed MoS<sub>2</sub> flake, the total dipole moment along the direction normal to the surface of MoS<sub>2</sub> is zero. (b) Separation of the centers (in black) of positive (in red) and negative charges (in blue) due to bending deformation.

284 the relaxed positions of a MoS<sub>2</sub> flake deformed under the action of an electric  
 285 field, using the QP model (Fig.4a). Then we compute the polarization for that  
 286 bent MoS<sub>2</sub> flake, for an hypothetical case where the charges of the sulfur atoms  
 287 would be the same in the upper and lower layers. In that hypothetical case, the  
 288 computation gives a polarization in the negative direction of  $z$  axis, whereas in the  
 289 undeformed MoS<sub>2</sub> flake, the total dipole moment along the out-of-plane direction

290 is always zero due to the fact that the molybdenum atomic layer is equidistantly  
 291 sandwiched between two layers of sulfur atoms. Fig.4b illustrates this phenomenon  
 292 with the case of the two rows of atoms nearest to the symmetry plane of the  
 293 deformed flake: the molybdenum cations are repelled away from the inner part  
 294 of the bend (which is its denser part). The consequence is that, while the charge  
 295 center of the sulfur anions stays half way between the two layers, the charge center  
 296 of the molybdenum is lower which results in a polarization pointing downwards  
 297 (hence a negative contribution to  $\mu_{3311}$  since  $G_{311}$  is positive in that case).

298 However, the above effect is not enough to fully account for the polarization  
 299 since we artificially used identical charges for the sulfur atoms. In reality, since  
 300 the overlapping of the electronic clouds of two nearby ions change during bending,  
 301 partial charges can be transferred from one sulfur layer to the other. In order to  
 302 understand that second contribution to the polarization, two representative areas  
 303 of the same deformed MoS<sub>2</sub> flake, named A and B, are considered in Fig.5a. The  
 304 average charge for the sulfur atoms in the upper and lower layers, calculated by  
 305 averaging net charges obtained by the QP model along  $y$  direction perpendicular  
 306 to the figure, are  $-0.776 e$  and  $-0.803 e$ , respectively. Therefore the atoms of the  
 307 lower sulfur layer appear to be more negative than those of the upper layer. This  
 308 creates a net dipole moment pointing from the outside to the inside of the curvature  
 309 (in the positive direction of  $z$  axis in our case). At the B site, the curvature is  
 310 much smaller than at the A site and consequently the difference in charges between  
 311 sulfur atoms in the upper and lower layer is smaller. In Fig.5b, we plotted the  
 312 average charge difference  $\Delta q = q_{lower} - q_{upper}$  between sulfur atoms in the lower and  
 313 upper layer, as a function of their index along the  $x$  coordinate (see numbers on the  
 314 molecular picture inside the graph). It can be seen that the absolute value of  $\Delta q$   
 315 decreases with the increasing index of sulfur, which agrees with what we expected  
 316 before implementing the computation, since it corresponds to the flexoelectric  
 317 effect: if the strain gradient is smaller, then the polarization is smaller (in absolute

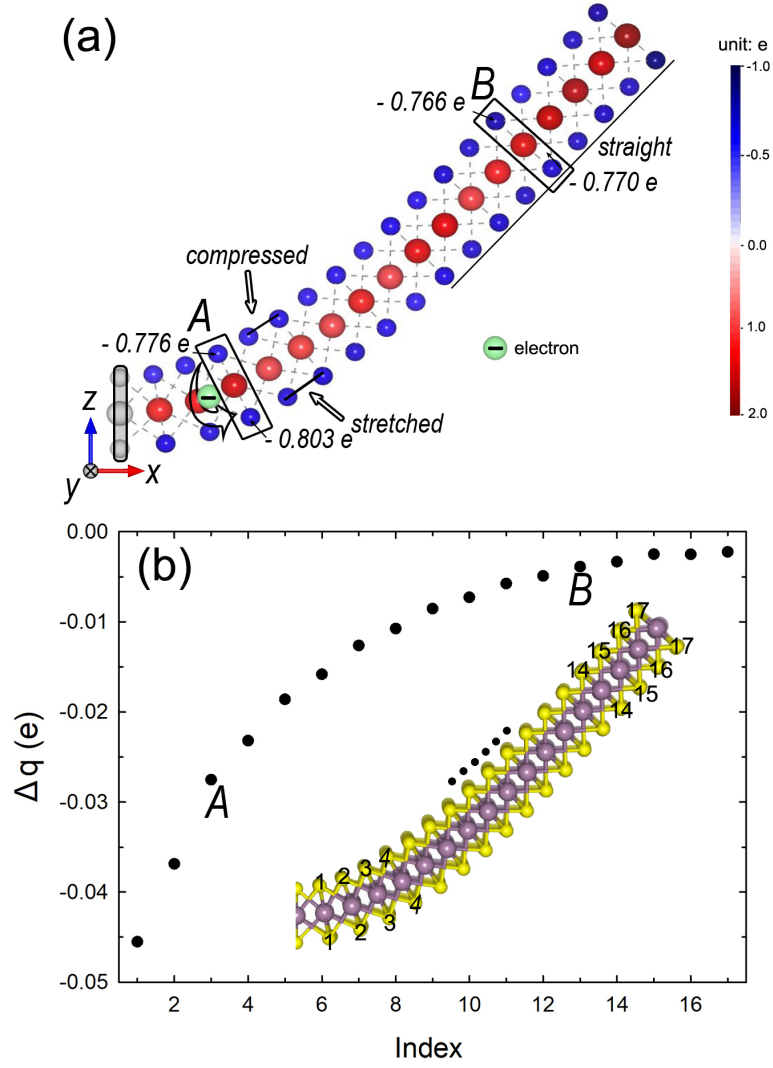


FIG. 5. (a) Charge distribution of a bent MoS<sub>2</sub> subjected to  $E_x = E_z = 0.4 \text{ V/\AA}$ .  $A$  and  $B$  are two representative regions for explanation of charges transfer from the upper layer to the lower layer, respectively. (b)  $\Delta q$  vs index.  $\Delta q$  is calculated as the charge of sulfur atoms in the lower layer minus the corresponding quantity for the upper layer. The upper and lower sulfur atoms are numbered by increasing value of  $z$ . Only the right portion of the bent MoS<sub>2</sub> is shown here.

318 value). Hence, we have two contributions in opposite directions: a downward  
 319 electric dipole moment due to bending of the lattice and an upward electric dipole  
 320 moment due to charge transfer. In the case of MoS<sub>2</sub>, our computations show  
 321 that polarization caused by bending deformation of lattice (which tends to give  
 322 a negative flexoelectric coefficient) surpasses that resulting from charge transfer  
 323 (which tends to give a positive flexoelectric coefficient). It is worth mentioning  
 324 here that a negative  $\mu_{3311}$  for MoS<sub>2</sub> monolayer has very recently been obtained  
 325 using first-principles linear-response theory<sup>71</sup>. Very interestingly, it can be found in  
 326 their calculations that two contributions coming from the dipolar and the lattice-  
 327 mediated response, respectively, to the total polarization response also play a  
 328 competing role, the signs of the former and the latter tending to be opposite, as  
 329 in our study.

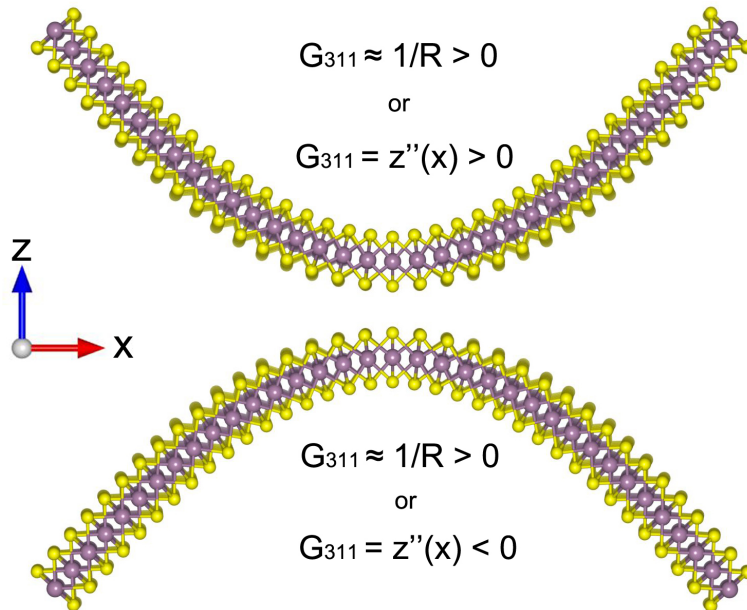


FIG. 6. Illustration of the different definitions for strain gradient  $G_{311}$ .

330 We now turn to the sign of the strain gradient. In a review paper, Wang et al<sup>72</sup>  
 331 pointed the discrepancies between definitions and symbols of physical quantities

332 to be one of the reasons for the inconsistency of the reported signs of flexoelectric  
333 coefficients. It is often the case for the strain gradient  $G_{311}$ . Indeed, on Fig.6  
334 we illustrate that the strain gradient, defined as  $G_{311} = u_z''(x)$  which can be either  
335 positive or negative, is often approximated as the inverse of the radius of curvature.  
336 Since, for some authors, the radius of curvature is always positive,  $G_{311}$  is always  
337 positive for them, regardless of the bending direction of the material. Slightly  
338 differently, Kundalwal et al<sup>48</sup> considered a boron nitride sheet shaped as an upward  
339 convex curved arch and defined  $G_{311}$  as the absolute value of the inverse of radius  
340 of curvature. We note, however, that we used a downward pointing bend (top part  
341 of Fig.6 and Fig.4) which gives a positive strain gradient for all these definitions.

342 The previous considerations tentatively explain why flexoelectric coefficients  
343 can be either positive or negative, due to a competition between lattice and charge  
344 transfer effect, and not always positive as some authors define it by using absolute  
345 values inside their definition.

### 346 C. In-plane flexoelectric coefficient $\mu_{1111}$ and $\mu_{2222}$

347 Inspired by the work of Hong et al<sup>73</sup>, the in-plane flexoelectric coefficients  $\mu_{1111}$   
348 and  $\mu_{2222}$  are computed in the present work. Strain gradient  $G_{111}$  is created by dis-  
349 placing every atoms along  $x$  axis, according to a parabolic displacement function  
350  $u_x(x)$ . Fig.7a is a schematic diagram showing the transverse displacement of atoms  
351 for a MoS<sub>2</sub> flake with a bigger (so that it be visible thanks to the two vertical lines)  
352 strain gradient imposed along  $x$  axis. Fig.7b shows the variation of displacement  
353 of atoms along  $x$  direction in the case  $\Delta d = u_x(x) = 0.01 - 10^{-5}x^2$ , strain  $\epsilon_{xx}$  and  
354 strain gradient  $\epsilon_{xx,x}$  ( $G_{111}$ ) as functions of the position along  $x$  axis for MoS<sub>2</sub>. We  
355 can see that the total strain is zero due to the symmetric distribution of displace-  
356 ment with respect to  $x = 0$ . Hence, the polarization due to piezoelectricity can be  
357 fully removed from the total polarization, leaving only flexoelectricity. Further-



358 more,  $\mu_{1111}$  can be expressed as  $\mu_{1111} = \frac{\partial P_1}{\partial G_{111}}$  and for a similar simulations with  
 359 parabolic displacement along  $y$ ,  $\mu_{2222} = \frac{\partial P_2}{\partial G_{222}}$ . The magnitude of strain gradient  
 360 for our calculations of  $\mu_{1111}$  and  $\mu_{2222}$  ranges from 0 to  $0.00004 \text{ \AA}^{-1}$ , which is small  
 361 enough to neglect any non-linear effect.

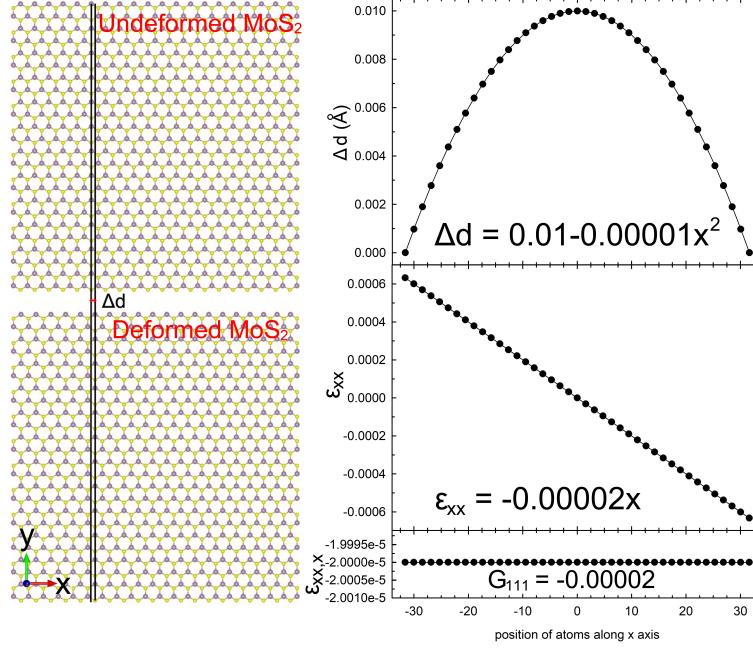


FIG. 7. (a) Applied displacement field along  $x$  axis for each atom with  $\Delta d$  denoting the  
 difference between the  $x$  coordinate of atoms in deformed MoS<sub>2</sub> and that in undeformed  
 MoS<sub>2</sub>. The two vertical lines are guides to the eye to see the displacements along  $x$   
 between the top and bottom sub-figures. (b) Displacement field  $\Delta d = u_x(x)$ , strain ( $\epsilon_{xx}$ )  
 and strain gradient ( $\epsilon_{xx,x} = G_{111}$ ) vs the position along  $x$  axis for MoS<sub>2</sub>.

362  
 363  
 364 The dependence of in-plane flexoelectric coefficients  $\mu_{1111}$  and  $\mu_{2222}$  on the width  
 365 of nanoribbon with infinite lengths is shown in [Figure 4 in Supplementary material](#).  
 366 Clearly, the in-plane flexoelectric coefficients increase as the width of nanoribbons  
 367 increases (polynomial fits are guides to the eye). The non-convergence behavior  
 368 of those flexoelectric coefficients with the increase of the width of the nanoribbons  
 369 has been elaborately discussed<sup>74</sup>. Hao et al. reveals through DFT calculations that

370 the flexoelectric coefficients of the 2D Janus TMDs nanoribbons depend strongly  
 371 upon their widths. The (slightly) different results for the two orientations are  
 372 probably due to edge effects different for armchair and zigzag edges. To completely  
 373 eliminate edge effect we use periodic boundary conditions in both directions for the  
 374 displacements. In their article,<sup>73</sup> Hong et al. computed the in-plane flexoelectric  
 375 coefficients of SrTiO<sub>3</sub> using a strain gradient with a cosine form, to be compatible  
 376 with the periodic boundary conditions. In our work, strain gradient is a constant  
 377 function (see Fig.7b), which is an even simpler case. Fig.8 shows the variations  
 378 of polarization  $P_1$  and  $P_2$  with strain gradient  $G_{111}$  and  $G_{222}$  for those doubly-  
 379 periodic setups. The computed flexoelectric coefficients  $\mu_{1111}$  and  $\mu_{2222}$  are 0.6872  
 380 nC/m and 0.7119 nC/m, respectively. Hence, the in-plane flexoelectric properties  
 381 of doubly-infinite MoS<sub>2</sub> are nearly isotropic, i.e. independent of the zigzag or  
 382 armchair direction.

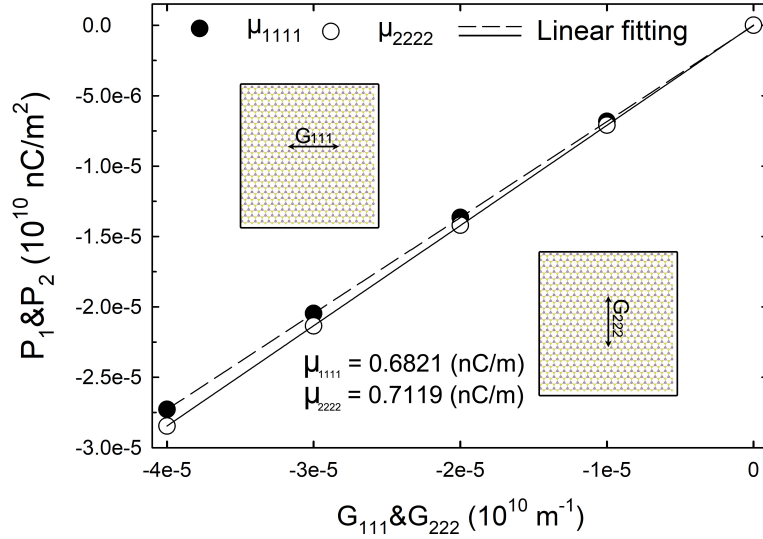


FIG. 8. Variations of polarization  $P_1$  and  $P_2$  with strain gradient  $G_{111}$  and  $G_{222}$ , respectively. The rectangular frame surrounding the edge of molybdenum disulfide represents the enforcement of periodic boundary conditions in both directions.

## 383 IV. CONCLUSIONS

384 Employing three different simulation setups, we calculated in-plane flexoelectric  
385 coefficients  $\mu_{1111}$ ,  $\mu_{2222}$ , transverse flexoelectric coefficient  $\mu_{3311}$  and out of plane  
386 flexoelectric coefficient  $\mu_{3333}$  for monolayer MoS<sub>2</sub> using the charge dipole model and  
387 charge conservation. The out-of-plane flexoelectric coefficient  $\mu_{3333}$  and transverse  
388 flexoelectric coefficient  $\mu_{3311}$  computed by the charge-dipole model are compared  
389 with those obtained by experimental measurements and DFT-based first principle  
390 calculations, by which good agreement in absolute value can be seen when the  
391 charge term is included in the computation of the polarization. We discuss in  
392 details possible origins of discrepancy in sign between our calculated flexoelectric  
393 coefficient  $\mu_{3311}$  and other reported results, by showing two opposite effects for the  
394 sign of the polarization. Furthermore, we emphasize that comparison of flexoelec-  
395 tric coefficients between different computational works requires a careful check for  
396 the sign of strain gradient and the way of defining the polarization. Concerning  
397 the computed in-plane flexoelectric coefficient  $\mu_{1111}$  and  $\mu_{2222}$  are found to be quasi  
398 identical, which is consistent with the analysis of symmetry for the flexoelectric  
399 coefficient tensor of a 2D continuum.

400 Finally, it is worth pointing out that the computed in-plane flexoelectric coef-  
401 ficient is about twenty times greater than out-of-plane flexoelectric coefficient for  
402 MoS<sub>2</sub>, which can be ascribed to the fact that the net charges induced by in-plane  
403 strain gradient between every primitive cells lead to the generation of larger electric  
404 dipole moments, whereas the movement of the charge in the out-of-plane direction  
405 is restricted due to the finite thickness. Hence, a relatively small polarization is  
406 then induced in the out-of-plane direction. **For 2D materials, bending seems to**  
407 **be the easiest way to externally generate a big strain gradient at nanoscale, on a**  
408 **large area. Therefore, even if in-plane flexoelectric coefficients may play a role in**  
409 **some systems, the differences between in-plane, out-of-plane and transverse coef-**  
410 **ficients in MoS<sub>2</sub> flakes is not big enough to compensate for the bigger and more**

411 homogeneous strain gradient that can be realized by bending. It is thus important  
412 to find 2D materials that optimize the transverse flexoelectric coefficients  $\mu_{3311}$  for  
413 applications in energy harvesting.

## 414 V. ACKNOWLEDGMENTS

415 This work was supported by the EIPHI Graduate School (contract "ANR-17-  
416 EURE-0002") and the Region of Bourgogne Franche-Comté (contract 2018-0054  
417 "ACTION  $\mu$ Mecatru. Computations have been performed on the supercomputer  
418 facilities of the Mésocentre de calcul de Franche-Comté.

## 419 VI. DATA AVAILABILITY

420 The data that support the findings of this study are available from the corre-  
421 sponding author upon reasonable request.

## 422 REFERENCES

- 423 <sup>1</sup>P. V. Yudin and A. K. Tagantsev, "Fundamentals of flexoelectricity in solids,"  
424 *Nanotechnology* **24**, 432001 (2013).
- 425 <sup>2</sup>Q. Deng, M. Kammoun, A. Erturk, and P. Sharma, "Nanoscale flexoelectric  
426 energy harvesting," *Int. J. Solids Struct.* **51**, 3218–3225 (2014).
- 427 <sup>3</sup>K. F. Wang and B. L. Wang, "Non-linear flexoelectricity in energy harvesting,"  
428 *Int. J. Eng. Sci.* **116**, 88–103 (2017).
- 429 <sup>4</sup>S. Zhang, K. Liu, M. Xu, and S. Shen, "A curved resonant flexoelectric actuator,"  
430 *Appl. Phys. Lett.* **111**, 082904 (2017).
- 431 <sup>5</sup>U. K. Bhaskar, N. Banerjee, A. Abdollahi, Z. Wang, D. G. Schlom, G. Rijnders,  
432 and G. Catalan, "A flexoelectric microelectromechanical system on silicon," *Nat.*  
433 *Nanotechnol.* **11**, 263–266 (2016).

- 434 <sup>6</sup>G. Dong, S. Li, M. Yao, Z. Zhou, Y.-Q. Zhang, X. Han, Z. Luo, J. Yao, B. Peng,  
435 Z. Hu, *et al.*, “Super-elastic ferroelectric single-crystal membrane with continuous  
436 electric dipole rotation,” *Science* **366**, 475–479 (2019).
- 437 <sup>7</sup>W. Huang, X. Yan, S. R. Kwon, S. Zhang, F.-G. Yuan, and X. Jiang, “Flexo-  
438 electric strain gradient detection using  $\text{Ba}_{0.64}\text{Sr}_{0.36}\text{TiO}_3$  for sensing,” *Appl. Phys.*  
439 *Lett.* **101**, 252903 (2012).
- 440 <sup>8</sup>S. Zhang, M. Xu, K. Liu, and S. Shen, “A flexoelectricity effect-based sensor for  
441 direct torque measurement,” *J. Phys. D: Appl. Phys.* **48**, 485502 (2015).
- 442 <sup>9</sup>V. S. Mashkevich and K. B. Tolpygo, “Electrical, optical and elastic properties  
443 of diamond type crystals,” *Sov. Phys. JETP* **5**, 435–439 (1957).
- 444 <sup>10</sup>S. M. Kogan, “Piezoelectric effect during inhomogeneous deformation and acous-  
445 tic scattering of carriers in crystals,” *Sov. Phys.-Solid State* **5**, 2069–2070 (1964).
- 446 <sup>11</sup>V. L. Indenbom, E. B. Loginov, and M. A. Osipov, “Flexoelectric effect and  
447 crystal-structure,” *Kristallografiya* **26**, 1157–1162 (1981).
- 448 <sup>12</sup>V. L. Indenbom, E. B. Loginov, and M. A. Osipov, “The flexoelectric effect and  
449 the structure of crystals,” *Sov Phys - Crystallogr.* **26**, 656–8 (1981).
- 450 <sup>13</sup>A. K. Tagantsev, “Theory of flexoelectric effect in crystals,” *Zh. Eksp. Teor. Fiz.*  
451 **88**, 2108–22 (1985).
- 452 <sup>14</sup>A. K. Tagantsev, “Piezoelectricity and flexoelectricity in crystalline dielectrics,”  
453 *Phys. Rev. B* **34**, 5883 (1986).
- 454 <sup>15</sup>E. Sahin and S. Dost, “A strain-gradients theory of elastic dielectrics with spatial  
455 dispersion,” *Int. J. Eng. Sci.* **26**, 1231–1245 (1988).
- 456 <sup>16</sup>P. Harris, “Mechanism for the shock polarization of dielectrics,” *J. Appl. Phys.*  
457 **36**, 739–741 (1965).
- 458 <sup>17</sup>A. Askar, P. C. Y. Lee, and A. S. Cakmak, “Lattice-dynamics approach to the  
459 theory of elastic dielectrics with polarization gradient,” *Phys. Rev. B* **1**, 3525–  
460 3537 (1970).

- 461 <sup>18</sup>R. Maranganti and P. Sharma, “Atomistic determination of flexoelectric proper-  
462 ties of crystalline dielectrics,” *Phys. Rev. B* **80**, 054109 (2009).
- 463 <sup>19</sup>R. Resta, “Towards a bulk theory of flexoelectricity,” *Phys. Rev. Lett.* **105**,  
464 127601 (2010).
- 465 <sup>20</sup>T. Dumitrică, C. M. Landis, and B. I. Yakobson, “Curvature induced polarization  
466 in carbon nanoshells,” *Chem. Phys. Lett.* **360**, 182–188 (2002).
- 467 <sup>21</sup>S. V. Kalinin and V. Meunier, “Electronic flexoelectricity in low-dimensional  
468 systems,” *Phys. Rev. B* **77**, 033403 (2008).
- 469 <sup>22</sup>I. Naumov, A. M. Bratkovsky, and V. Ranjan, “Unusual flexoelectric effect in two-  
470 dimensional noncentrosymmetric  $sp^2$ -bonded crystals,” *Phys. Rev. Lett.* **102**,  
471 217601 (2009).
- 472 <sup>23</sup>P. J. Mitchell and D. Fincham, “Shell model simulations by adiabatic dynamics,”  
473 *J. Phys. Condens. Matter* **5**, 1031 (1993).
- 474 <sup>24</sup>M. S. Majdoub, P. Sharma, and T. Cagin, “Enhanced size-dependent piezoelec-  
475 tricity and elasticity in nanostructures due to the flexoelectric effect,” *Phys. Rev.*  
476 *B* **77**, 125424 (2008).
- 477 <sup>25</sup>R. Mbarki, J. B. Haskins, A. Kinaci, and T. Cagin, “Temperature dependence  
478 of flexoelectricity in  $\text{BaTiO}_3$  and  $\text{SrTiO}_3$  perovskite nanostructures,” *Phys. Lett. A*  
479 **378**, 2181–2183 (2014).
- 480 <sup>26</sup>A. Chatzopoulos, P. Beck, J. Roth, and H.-R. Trebin, “Atomistic modeling of  
481 flexoelectricity in periclase,” *Phys. Rev. B* **93**, 024105 (2016).
- 482 <sup>27</sup>S. Mao, P. K. Purohit, and N. Aravas, “Mixed finite-element formulations in  
483 piezoelectricity and flexoelectricity,” *Proc. R. Soc. A: Math. Phys. Eng. Sci.* **472**,  
484 20150879 (2016).
- 485 <sup>28</sup>Y. Mao, S. Ai, X. Xiang, and C. Chen, “Theory for dielectrics considering the  
486 direct and converse flexoelectric effects and its finite element implementation,”  
487 *Appl. Math. Model.* **40**, 7115–7137 (2016).

- 488 <sup>29</sup>H. T. Chen, A. K. Soh, and Y. Ni, “Phase field modeling of flexoelectric effects  
489 in ferroelectric epitaxial thin films,” *Acta Mech.* **225**, 1323–1333 (2014).
- 490 <sup>30</sup>Q. Li, C. T. Nelson, S.-L. Hsu, A. R. Damodaran, L.-L. Li, A. K. Yadav, M. Mc-  
491 Carter, L. W. Martin, R. Ramesh, and S. V. Kalinin, “Quantification of flexo-  
492 electricity in PbTiO<sub>3</sub>/SrTiO<sub>3</sub> superlattice polar vortices using machine learning  
493 and phase-field modeling,” *Nat. Commun.* **8**, 1–8 (2017).
- 494 <sup>31</sup>K. M. Hamdia, H. Ghasemi, X. Zhuang, N. Alajlan, and T. Rabczuk, “Computa-  
495 tional machine learning representation for the flexoelectricity effect in truncated  
496 pyramid structures,” *Comput. Mater. Contin.* **59**, 79–87 (2019).
- 497 <sup>32</sup>L. Xiang, X. Zeng, X. Huang, and G. Li, “The application of artificial neural-  
498 network potentials for flexoelectricity: Performance for anatase-type TiO<sub>2</sub>,”  
499 *Phys. Lett. A* **384**, 126217 (2020).
- 500 <sup>33</sup>H. Ghasemi, H. S. Park, and T. Rabczuk, “A multi-material level set-based  
501 topology optimization of flexoelectric composites,” *Computer Methods in Ap-  
502 plied Mechanics and Engineering* **332**, 47–62 (2018).
- 503 <sup>34</sup>H. V. Do, T. Lahmer, X. Zhuang, N. Alajlan, H. Nguyen-Xuan, and T. Rabczuk,  
504 “An isogeometric analysis to identify the full flexoelectric complex material prop-  
505 erties based on electrical impedance curve,” *Computers & Structures* **214**, 1–14  
506 (2019).
- 507 <sup>35</sup>W. Ma and L. E. Cross, “Large flexoelectric polarization in ceramic lead magne-  
508 sium niobate,” *Appl. Phys. Lett.* **79**, 4420–4422 (2001).
- 509 <sup>36</sup>W. Ma and L. E. Cross, “Observation of the flexoelectric effect in relaxor  
510 Pb(Mg<sub>1/3</sub>Nb<sub>2/3</sub>)O<sub>3</sub> ceramics,” *Appl. Phys. Lett.* **78**, 2920–2921 (2001).
- 511 <sup>37</sup>W. Ma and L. E. Cross, “Flexoelectric polarization of barium strontium titanate  
512 in the paraelectric state,” *Appl. Phys. Lett.* **81**, 3440–3442 (2002).
- 513 <sup>38</sup>W. Ma and L. E. Cross, “Strain-gradient-induced electric polarization in lead  
514 zirconate titanate ceramics,” *Appl. Phys. Lett.* **82**, 3293–3295 (2003).

515 <sup>39</sup>W. Ma and L. E. Cross, “Flexoelectric effect in ceramic lead zirconate titanate,”  
516 Appl. Phys. Lett. **86**, 072905 (2005).

517 <sup>40</sup>W. Ma and L. E. Cross, “Flexoelectricity of barium titanate,” Appl. Phys. Lett.  
518 **88**, 232902 (2006).

519 <sup>41</sup>J. Narvaez and G. Catalan, “Origin of the enhanced flexoelectricity of relaxor  
520 ferroelectrics,” Appl. Phys. Lett. **104**, 162903 (2014).

521 <sup>42</sup>L. Shu, W. Huang, S. Ryung Kwon, Z. Wang, F. Li, X. Wei, S. Zhang, M. Lan-  
522 gan, X. Yao, and X. Jiang, “Converse flexoelectric coefficient  $f_{1212}$  in bulk  
523  $\text{Ba}_{0.67}\text{Sr}_{0.33}\text{TiO}_3$ ,” Appl. Phys. Lett. **104**, 232902 (2014).

524 <sup>43</sup>W. Huang, K. Kim, S. Zhang, F.-G. Yuan, and X. Jiang, “Scaling effect of  
525 flexoelectric  $(\text{Ba}, \text{Sr})\text{TiO}_3$  microcantilevers,” Phys. Status Solidi Rapid Res. Lett.  
526 **5**, 350–352 (2011).

527 <sup>44</sup>A. Kvashnin, P. Sorokin, and B. Yakobson, “Flexoelectricity in carbon nanostruc-  
528 tures: Nanotubes, fullerenes, and nanocones,” J. Phys. Chem. Lett. **6**, 2740–4  
529 (2015).

530 <sup>45</sup>S. Chandratre and P. Sharma, “Coaxing graphene to be piezoelectric,” Appl.  
531 Phys. Lett. **100**, 023114 (2012).

532 <sup>46</sup>S. I. Kundalwal, S. A. Meguid, and G. J. Weng, “Strain gradient polarization in  
533 graphene,” Carbon **117**, 462–472 (2017).

534 <sup>47</sup>T. Pandey, L. Covaci, M. V. Milošević, and F. M. Peeters, “Flexoelectricity and  
535 transport properties of phosphorene nanoribbons under mechanical bending,”  
536 Phys. Rev. B **103**, 235406 (2021).

537 <sup>48</sup>S. I. Kundalwal, V. K. Choyal, and V. Choyal, “Flexoelectric effect in boron  
538 nitride–graphene heterostructures,” Acta Mech. **232**, 3781–3800 (2021).

539 <sup>49</sup>W. Shi, Y. Guo, Z. Zhang, and W. Guo, “Flexoelectricity in monolayer transition  
540 metal dichalcogenides,” J. Phys. Chem. Lett. **9**, 6841–6846 (2018).

541 <sup>50</sup>W. Shi, Y. Guo, Z. Zhang, and W. Guo, “Strain gradient mediated magnetism  
542 and polarization in monolayer  $\text{vse}_2$ ,” J. Phys. Chem. C **123**, 24988–24993 (2019).



543 <sup>51</sup>S. Kumar, D. Codony, I. Arias, and P. Suryanarayana, “Flexoelectricity in atomic  
544 monolayers from first principles,” *Nanoscale* **13**, 1600–1607 (2021).

545 <sup>52</sup>X. Zhuang, B. He, B. Javvaji, and H. S. Park, “Intrinsic bending flexoelectric  
546 constants in two-dimensional materials,” *Phys. Rev. B* **99**, 054105 (2019).

547 <sup>53</sup>B. Javvaji, B. He, X. Zhuang, and H. S. Park, “High flexoelectric constants in  
548 Janus transition-metal dichalcogenides,” *Phys. Rev. Mater.* **3**, 125402 (2019).

549 <sup>54</sup>Z. Wang and M. Devel, “Electrostatic deflections of cantilevered metallic carbon  
550 nanotubes via charge-dipole model,” *Phys. Rev. B* **76**, 195434 (2007).

551 <sup>55</sup>Z. Wang, M. Zdrojek, T. Mélin, and M. Devel, “Electric charge enhancements in  
552 carbon nanotubes: Theory and experiments,” *Phys. Rev. B* **78**, 085425 (2008).

553 <sup>56</sup>Y. Yang, M. Devel, and Z. Wang, “An atomistic model for the charge distribution  
554 in layered MoS<sub>2</sub>,” *J. Chem. Phys.* **149**, 124102 (7) (2018).

555 <sup>57</sup>C. J. Brennan, R. Ghosh, K. Koul, S. K. Banerjee, N. Lu, and E. T. Yu, “Out-of-  
556 plane electromechanical response of monolayer molybdenum disulfide measured  
557 by piezoresponse force microscopy,” *Nano Lett.* **17**, 5464–5471 (2017).

558 <sup>58</sup>C. J. Brennan, K. Koul, N. Lu, and E. T. Yu, “Out-of-plane electromechanical  
559 coupling in transition metal dichalcogenides,” *Appl. Phys. Lett.* **116**, 053101  
560 (2020).

561 <sup>59</sup>M. L. Olson and K. R. Sundberg, “An atom monopole–dipole interaction model  
562 with charge transfer for the treatment of polarizabilities of  $\pi$ -bonded molecules.”  
563 *J. Chem. Phys.* **69**, 5400–5404 (1978).

564 <sup>60</sup>A. Mayer, P. Lambin, and R. Langlet, “Charge-dipole model to compute the  
565 polarization of fullerenes,” *Appl. Phys. Lett.* **89**, 063117 (2006).

566 <sup>61</sup>A. Mayer, “Formulation in terms of normalized propagators of a charge-dipole  
567 model enabling the calculation of the polarization properties of fullerenes and  
568 carbon nanotubes,” *Phys. Rev. B* **75**, 045407 (2007).

569 <sup>62</sup>A. Mayer and P.-O. Åstrand, “A charge-dipole model for the static polarizability  
570 of nanostructures including aliphatic, olephinic, and aromatic systems,” *J. Phys.*

571 Chem. A **112**, 1277–1285 (2008).

572 <sup>63</sup>A. Mayer, A. L. Gonzalez, C. M. Aikens, and G. C. Schatz, “A charge–dipole  
573 interaction model for the frequency-dependent polarizability of silver clusters,”  
574 Nanotechnology **20**, 195204 (2009).

575 <sup>64</sup>L. Jensen, P. O. Åstrand, A. Osted, J. Kongsted, and K. V. Mikkelsen, “Polar-  
576 izability of molecular clusters as calculated by a dipole interaction model,” J.  
577 Chem. Phys. **116**, 4001–4010 (2002).

578 <sup>65</sup>R. Langlet, M. Devel, and P. Lambin, “Computation of the static polarizabilities  
579 of multi-wall carbon nanotubes and fullerenes using a Gaussian regularized point  
580 dipole interaction model,” Carbon **44**, 2883–2895 (2006).

581 <sup>66</sup>X. Li and H. Zhu, “Two-dimensional MoS<sub>2</sub>: Properties, preparation, and appli-  
582 cations,” J. Materiomics **1**, 33–44 (2015).

583 <sup>67</sup>M. Wen, S. N. Shirodkar, P. Plecháč, E. Kaxiras, R. S. Elliott, and E. B. Tadmor,  
584 “A force-matching Stillinger-Weber potential for MoS<sub>2</sub>: Parameterization and  
585 Fisher information theory based sensitivity analysis,” J. Appl. Phys. **122**, 244301  
586 (2017).

587 <sup>68</sup>M. Madziarz, “Transferability of molecular potentials for 2D molybdenum disul-  
588 phide,” Materials **14**, 519 (2021).

589 <sup>69</sup>H. Hirakata, Y. Fukuda, and T. Shimada, “Flexoelectric properties of multilayer  
590 two-dimensional material MoS<sub>2</sub>,” J. Phys. D: Appl. Phys. **55**, 125302 (2021).

591 <sup>70</sup>Y. Lee, S. Park, H. Kim, G. H. Han, Y. H. Lee, and J. Kim, “Characteriza-  
592 tion of the structural defects in CVD-grown monolayered MoS<sub>2</sub> using near-field  
593 photoluminescence imaging,” Nanoscale **7**, 11909–11914 (2015).

594 <sup>71</sup>M. Springolo, M. Royo, and M. Stengel, “Direct and converse flexoelectricity in  
595 two-dimensional materials,” Phys. Rev. Lett. **127**, 216801 (2021).

596 <sup>72</sup>B. Wang, Y. Gu, S. Zhang, and L.-Q. Chen, “Flexoelectricity in solids: Progress,  
597 challenges, and perspectives,” Prog. Mater. Sci **106**, 100570 (2019).

598 <sup>73</sup>J. Hong, G. Catalan, J. F. Scott, and E. Artacho, “The flexoelectricity of barium  
599 and strontium titanates from first principles,” *J. Phys. Condens. Matter* **22**,  
600 112201 (2010).

601 <sup>74</sup>W. Hao, Z. Wu, X. Li, and Y. Pu, “Edge effect on flexoelectronic properties of  
602 Janus MoSSe nanoribbons: A first-principles study,” *J. Appl. Phys.* **129**, 185101  
603 (2021).